^{20}F from the ^{13}C(^{11}B,α)^{20}F reaction

G.-B. Liu and H. T. Fortune
Physics Department, University of Pennsylvania, Philadelphia, Pennsylvania 19104
(Received 22 June 1988)

The ^{13}C(^{11}B,α)^{20}F and ^{11}B(^{13}C,α)^{20}F reactions have been used to populate states in ^{20}F up to 10.1 MeV excitation. Angular distributions and total cross sections have been extracted and compared with Hauser-Feshbach calculations. Agreement is reasonable for most states. A few states appear to be populated by an additional reaction mechanism. Candidates for high-spin states are compared with those calculated in weak coupling with $(4+n)$p-nh configurations. The present results are compared with results of the ^{14}N(^{7}Li,p)^{20}F reaction. The correlation coefficient between the two sets of angle-integrated cross sections is 0.88.

I. INTRODUCTION

Many types of reactions have been used to study ^{20}F. One-, two-, and three-nucleon direct-transfer reactions[1–10] provided a great deal of spectroscopic information. Compound reactions such as (d,α),[11] (^{7}Li,p),[12–14] (^{9}Be,d),[15] and (^{11}B,α) (Ref. 16) were carried out to get knowledge of the nuclear structure of ^{20}F. The (^{7}Li,^{3}He) (Ref. 17) reaction was found to proceed by a mixture of direct and compound mechanisms. Much information concerning ^{20}F is summarized in a recent compilation.[18]

Wildenthal's $(sd)^4$ calculation[19] predicted many high-spin states below 11 MeV in ^{20}F, and weak-coupling calculations for 5p-1h, 6p-2h, 7p-3h, and 8p-4h configurations produce many more high-spin states in this range of excitation. Recently, we published a paper on ^{21}Ne(t,α)^{20}F reaction[20] and provided spectroscopic information on ^{20}F up to 4.1 MeV. The purpose of the present heavy-ion experiment is to populate states at much higher excitations (up to 10.1 MeV). We compare the results with Hauser-Feshbach (HF) calculations and with experimental results from the ^{14}N(^{7}Li,p)^{20}F reaction.[13,14] Candidates for high-J states are identified and compared with those expected from weak-coupling and $(sd)^4$ shell-model calculations.

II. EXPERIMENTAL PROCEDURE

The experiments were performed with a 22.0-MeV ^{11}B beam and a 26.0-MeV ^{13}C beam from the University of Pennsylvania tandem accelerator. The ^{13}C target was a 10-μg/cm^2 foil and the ^{11}B target 20 μg/cm^2. The outgoing α particles were momentum analyzed in a multiangle spectrograph and detected in nuclear emulsion plates. Data were recorded at 12 laboratory angles from 3.75° to 93.75° in steps of 7.5° for the ^{13}C(^{11}B,α) reaction and at two laboratory angles (3.75° and 11.25°) for the ^{11}B(^{13}C,α) reaction. Some data points are missing for some states due mainly to impurity contributions. Because data at angle θ in the ^{11}B(^{13}C,α) reaction correspond to ones at $(\pi-\theta)$ in the complementary ^{13}C(^{11}B,α) reaction, we discuss only the latter reaction, and forward-angle data from the former reaction are treated as backward angle.

A spectrum of α particles from ^{13}C(^{11}B,α)^{20}F is displayed in Fig. 1. The typical resolution is about 52 keV FWHM. Sixty peaks in the figure were identified, of which at least 32 are known to be doublets or multiplets. In Fig. 2 an α spectrum from ^{11}B(^{13}C,α)^{20}F is shown. Its typical resolution is about 124 keV. Integrated cross sections $\sigma_{\rm exp}$ were calculated from the differential cross sections with the help of the computer code LEGFIT.[21] Table I lists results of the present work together with previous information on ^{20}F levels. The last column of the table lists the ratios σ_B/σ_F of differential cross sections at backward and forward angles. When data exist at two backward angles, the ratio is taken after summing the two angles. In Figs. 3–11 angular distributions of the ^{13}C(^{11}B,α)^{20}F reaction are shown.

Our excitation energies are in generally good agreement with values from the compilation. Up to 4.1 MeV, 15 of our peaks presumably correspond to single states. For those levels, the standard deviation between our values of E_x and those in the compilation is 2 keV. Above this energy most of our peaks are doublets or multiplets, and it is therefore more difficult to compare excitation energies. However, in a few cases, our value of E_x differs sufficiently from the known one (as, e.g., the known state at 5.224 MeV and our E_x of 5.255 MeV) to indicate that the state we observe is not the one previously known. This suggestion is strengthened by the magnitude of the total cross section.

III. ANALYSIS AND DISCUSSION

Compound-nuclear contributions to the reaction mechanism have been calculated with the computer code STATIS[22] using the Hauser-Feshbach formalism.[23] Reactions of the type (HI,α) are powerful tools to investigate nuclear structure of residual nuclei. Reactions such as ^{14}N(^{14}N,α)^{24}Mg,[24] ^{14}N(^{12}C,α)^{22}Na,[25,26] have been used to populate levels of the residual nuclei, and results for

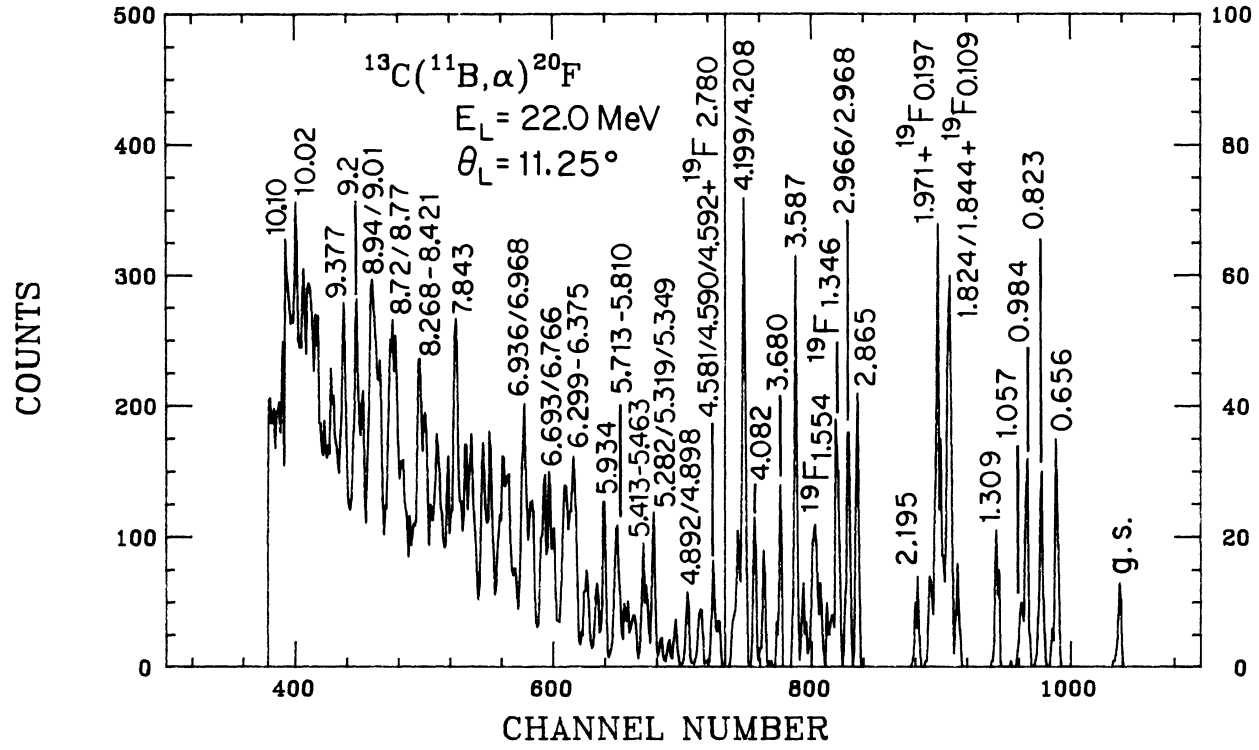

FIG. 1. Spectrum of alpha particles from the reaction ^{13}C(^{11}B,α)^{20}F reaction, at E(^{11}B)=22.0 MeV and a laboratory angle of 11.25°. States in ^{20}F are labeled by their excitation energies. Peaks from impurities in the target are hatched and labeled by final nucleus and excitation energy.

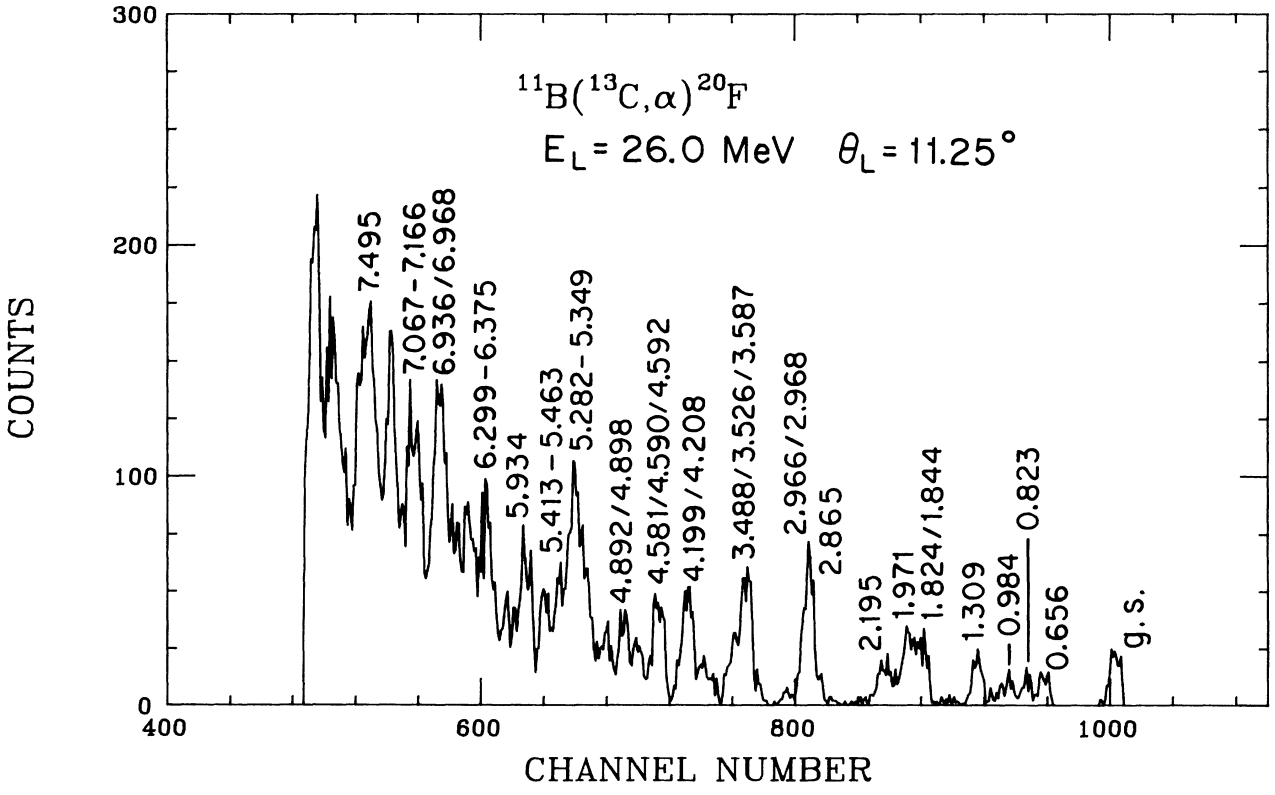

FIG. 2. Spectrum of alpha particles from the reaction ^{11}B(^{13}C,α)^{20}F reaction, at E(^{13}C)=26.0 MeV and θ_l=11.25°.

TABLE I. Results of present experiment and comparison with previous information concerning ^{20}F.

Previous[a]		Present				
E_x (MeV)	J^π	E_x (MeV±keV)	σ_{exp} (mb)	$J\pm\delta J$	σ_{HF} (mb)	σ_B/σ_F
0.000	2^+	−0.003±5	0.249	2.09±0.46	0.214	1.545
0.656	3^+	0.658±4	0.299	2.61±0.56	0.280	1.161
0.823	4^+	0.819±4	0.430	3.98±0.80	0.456	0.776
0.984	1^-	0.986±6	0.173	1.30±0.32	0.107	0.724
1.057	1^+	1.038±10	0.123	0.78±0.23	0.097	0.585
1.309	2^-	1.307±4	0.304	2.67±0.57	0.168	1.146
1.824	5^+	1.823±7	0.965	9.05±1.80	0.543	0.624
1.844	2^-				0.158	
1.971	3^-	1.979±5	0.561	5.34±1.05	0.266	0.629
2.044	2^+	2.053±9	0.262	2.23±0.49	0.168	1.065
2.195	3^+	2.195±5	0.309	2.72±0.58	0.236	2.163
2.865	3^-	2.868±6	0.380	3.46±0.71	0.239	1.679
2.966	3^+	2.968±6	0.804	7.38±1.50	0.215	3.574
2.968	4^-				0.317	
3.173	1^+	3.174±10	0.151	1.07±0.28	0.072	0.810
3.488	1^+	3.493±6	0.138	0.44±0.26	0.0688	6.487
3.526	0^+				0.0217	
3.587	$(1,2,3,)^+$	3.590±4	0.620	5.46±1.16	0.199(3^+),0.136(2^+)	1.000
3.680	3^++1^-	3.670±5	0.564	4.88±1.05	0.197+0.070	0.740
	5^++0^-				0.424+0.021	
3.761	$(2^-,3^+)$	3.753±6	0.332	2.96±0.62	0.122,0.195	2.298
3.965	1^+	3.966±7	0.126	0.81±0.24	0.064	0.941
4.082	$(1)^+$	4.076±7	0.155	1.11±0.29	0.063	1.743
4.199		4.200±6	0.800	7.33±1.49		0.980
4.208						
4.277	(1,2)				0.123(2^+)	
4.315	$(0,1)^+$	4.285±7	0.221	1.30±0.41	0.019(0^+),0.061(1^+)	2.099
4.371	(2^+)				0.121	
4.509	$1^+(2)$	4.511±7	0.609	5.84±1.14	0.059(1^+)	1.462
4.511[b]	$(6^+,4^-)$				0.690(6^+),0.264(4^-)	
4.581						
4.590[c]		4.577±5	0.753	6.34±1.41	1.018	0.747
4.592						
4.731	$(3^-,4,5^+)$	4.745±4	0.713	6.43±1.33	0.372(5^+),0.283(4^+)	0.688
4.766						
4.892		4.885±5	0.470	3.90±0.88		1.128
4.898						
5.047	(2^-)	5.060±10	0.474	3.94±0.88	0.101(2^-)	1.532
5.068	$(1^-,2,3^+)$				0.163(3^+)	
5.131	$(2^-,3,4^+)$	5.127±4	0.322	2.85±0.60	0.268(4^+)	0.631
5.224	$(1,2)^-$	5.255±15	0.681	6.59±1.27	0.0526,0.0997	
5.282						
5.319	0,1,2	5.317±6	1.282	11.85±2.39	0.103(2^+),0.096(2^-)	0.849
5.349	(3^+)				0.157	
5.413						
5.450		5.420±7	1.960	18.42±3.66		1.515
5.455						
5.463	$(1,2,3)^+$				0.154(3^+)	
5.555	$1,2^+$				0.049(1^+)0.098(2^+)	
5.588		5.574±6	0.707	5.86±1.32		1.186
5.620						
5.713						
5.764	$(3)^+$	5.753±6	0.655	5.32±1.22	0.147	0.442
5.810	(1^+)				0.046	
5.936	2^-	5.934±14	1.470	14.81±2.74	0.086	0.382
6.018	2^-				0.085	
6.045	0,1,2,	6.008±15	0.864	7.50±1.61	0.089(2^+),0.084(2^-)	1.066
6.090	(0^-)				0.013	
6.161	$(2,3^+)$				0.087(2^+),0.138(3^+)	

TABLE I. (*Continued*)

Previous[a]		Present				
E_x (MeV)	J^π	E_x (MeV±keV)	σ_{exp} (mb)	$J\pm\delta J$	σ_{HF} (mb)	σ_B/σ_F
6.200	(2$^-$,3,4$^+$)	6.164±16	0.722	6.52±1.35	0.230(4$^+$),0.137(3$^+$)	0.216
6.240						
6.299						
6.339		6.353±12	0.891	7.78±1.66		0.108
6.375						
6.416						
6.441		6.453±16	1.483	14.45±2.77		0.694
6.474						
6.519	0$^+$;$T=2$					
6.588						
6.627	2$^-$	6.611±13	1.244	10.96±2.32	0.077	0.521
6.643	(3,4)				0.216(4$^+$),0.127(3$^+$)	
6.648	1$^-$				0.039	
6.693	1$^-$	6.691±5	1.228	11.79±2.29	0.039	
6.766	(2$^-$,3,4$^+$)				0.212(4$^+$),0.125(3$^+$)	
6.825						
6.857	2	6.860±8	1.238	11.40±2.31	0.076(2$^+$),0.074(2$^-$)	0.463
6.905						
6.936		6.962±9	2.300	22.96±4.29		1.042
6.968	1$^-$				0.037	
(7.067)	0$^-$				0.011	
7.08	(1$^+$)	7.178±12	1.345	13.01±2.51	0.036	0.485
7.166	2$^{(+)}$				0.072	
7.232						
7.283		7.280±10	1.452	14.13±2.71		0.577
7.319	(1)				0.034(1$^+$)	
7.37	(1)	7.420±7	0.871	8.07±1.63	0.034(1$^+$)	
7.42	(2$^+$)				0.069	
7.495	(2)	7.498±10	1.017	10.09±1.90	0.067(2$^+$),0.065(2$^-$)	0.829
7.655	(2$^+$)	7.674±16	1.357	13.64±2.53	0.065	
7.734		7.767±18	1.747	17.70±3.26		
7.843	1$^-$	7.859±8	2.425	24.76±4.53	0.031	
7.985	1	7.976±13	1.420	14.29±2.65	0.030(1$^+$),0.029(1$^-$)	
8.05	2$^+$;$T=2$					
8.062						
8.113		8.133±8	1.696	16.17±3.17		
8.147						
8.268						
8.349		8.332±10	2.739	27.03±5.11		
8.421						
8.50						
		8.579±21	0.833	8.18±1.55		
8.72		8.717±10	3.016	30.42±5.63		
8.77						
8.94		8.974±17	3.519	36.16±6.57		
9.01		9.119±8	1.458	14.69±2.72		
9.2		9.212±6	1.709	17.30±3.19		
		9.377±9	1.608	16.25±3.00		
9.52		9.587±13	1.142	10.90±2.13		
9.65						
9.83						
9.85		9.845±18	1.558	14.73±2.91		
(9.886)						
9.90		9.918±9	2.199	21.91±4.10		
(9.929)						
(9.981)		10.043±11	2.702	27.16±5.04		
10.024						
10.10		10.180±10	2.212	22.04±4.13		
10.228						

[a]Reference 18. [b]Reference 13. [c]Reference 14.

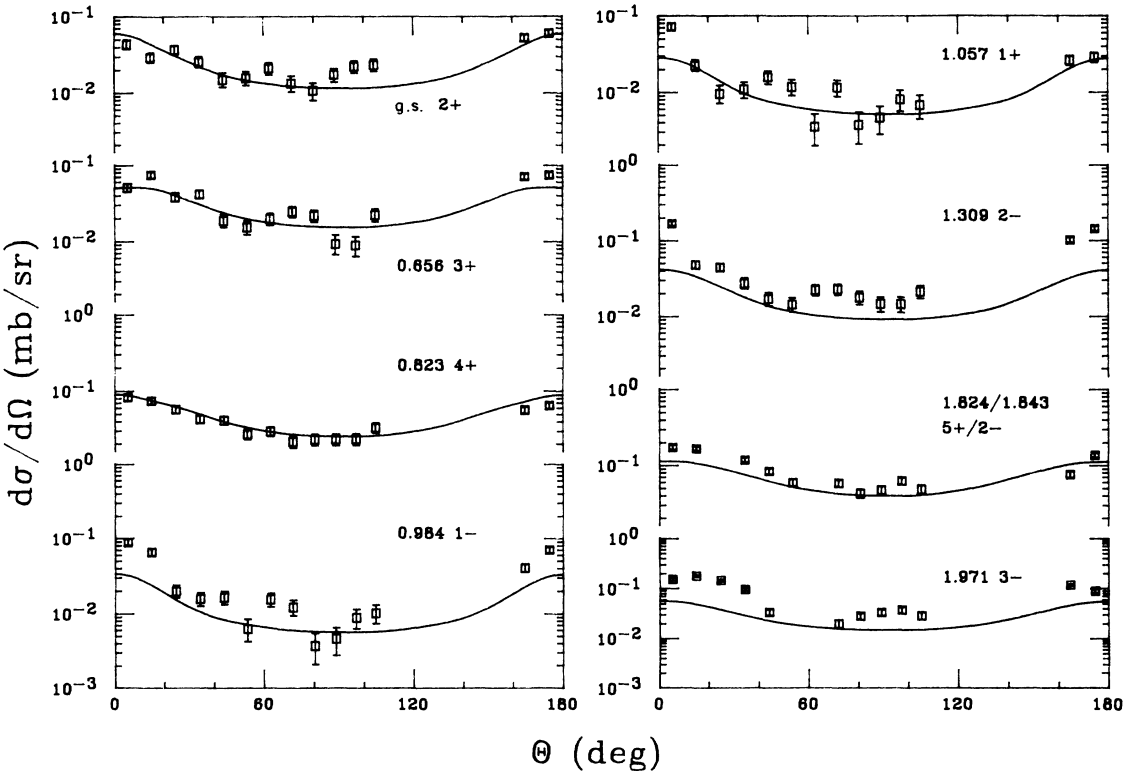

FIG. 3. Angular distributions for the reaction $^{13}C(^{11}B,\alpha)^{20}F$, compared with HF curves.

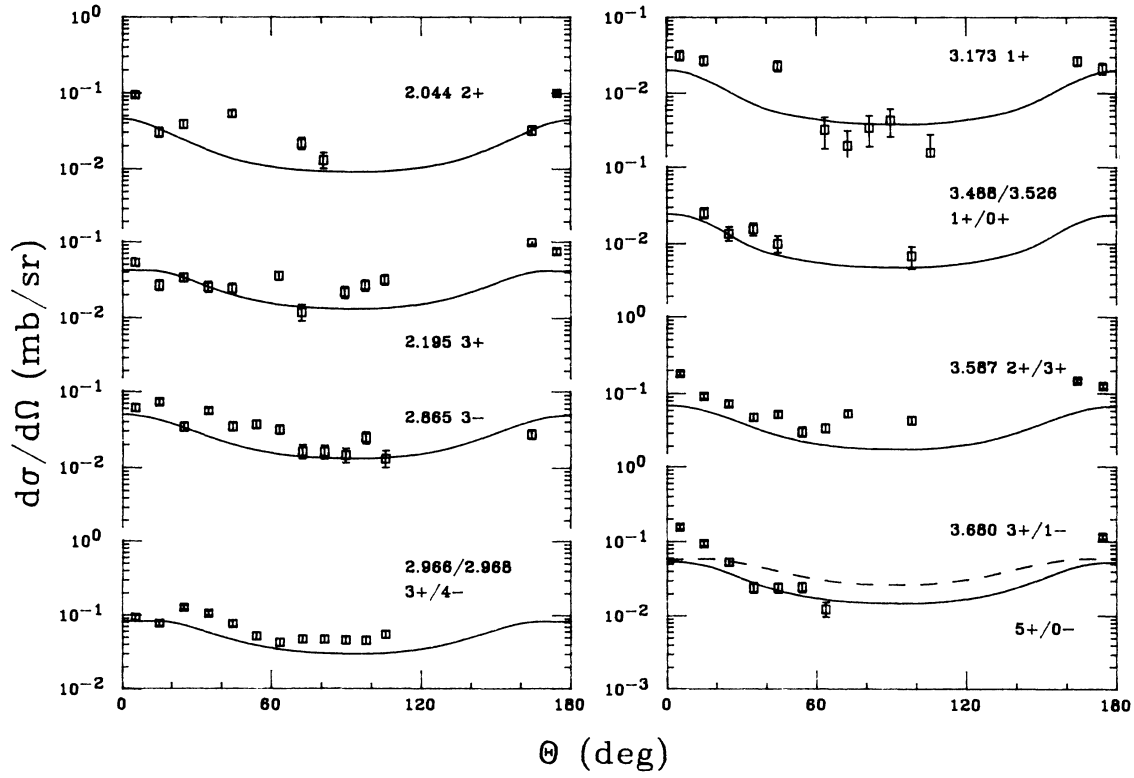

FIG. 4. Same as Fig. 3, but for $E_x = 2.0-3.6$ MeV.

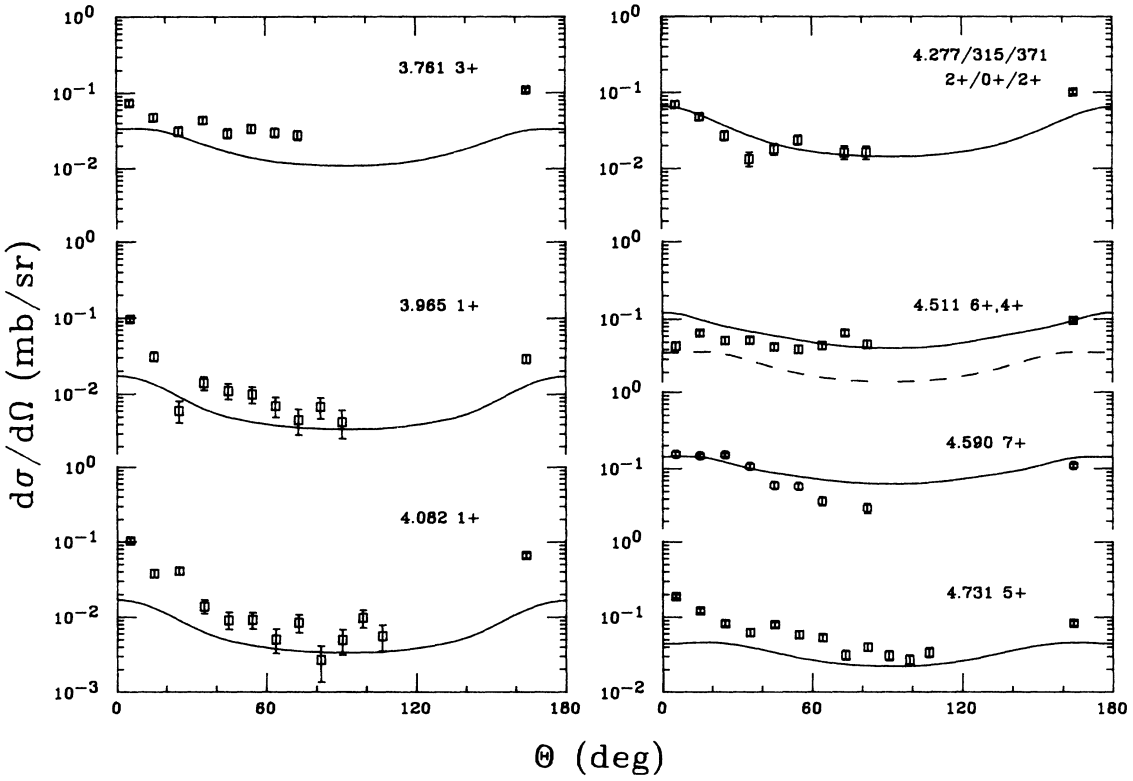

FIG. 5. Same as Fig. 3, but for $E_x = 3.7$–4.7 MeV.

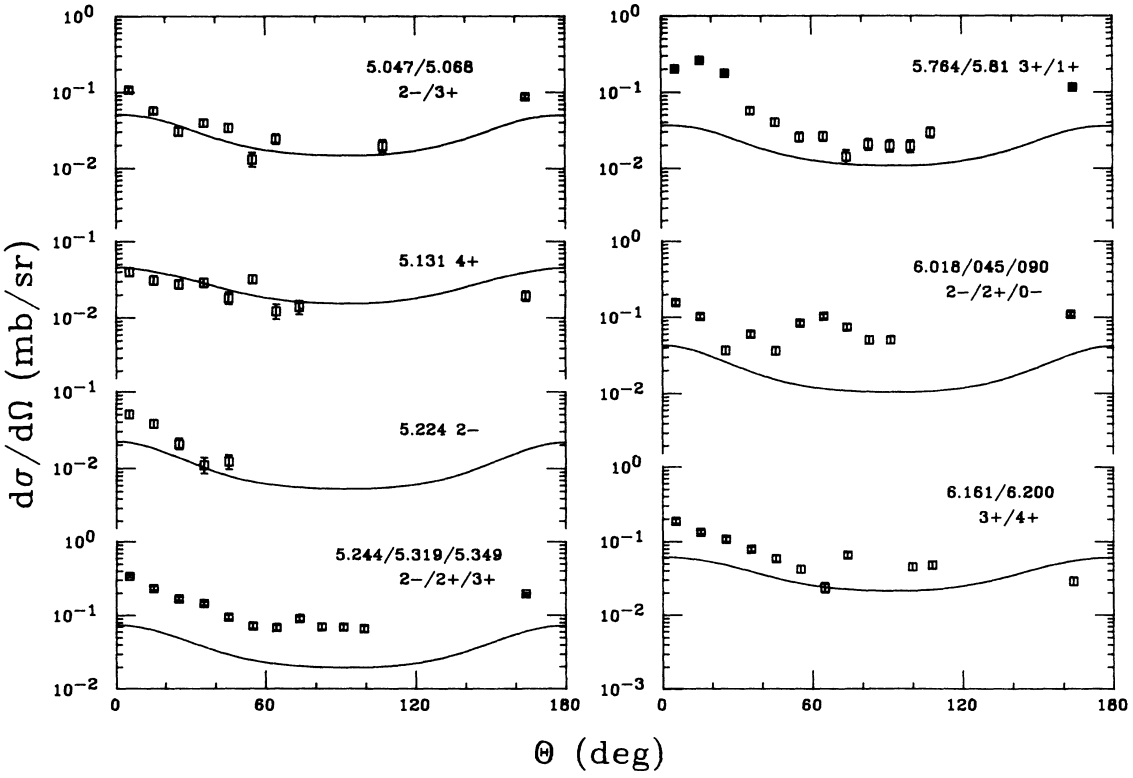

FIG. 6. Same as Fig. 3, but for $E_x = 5.0$–6.2 MeV.

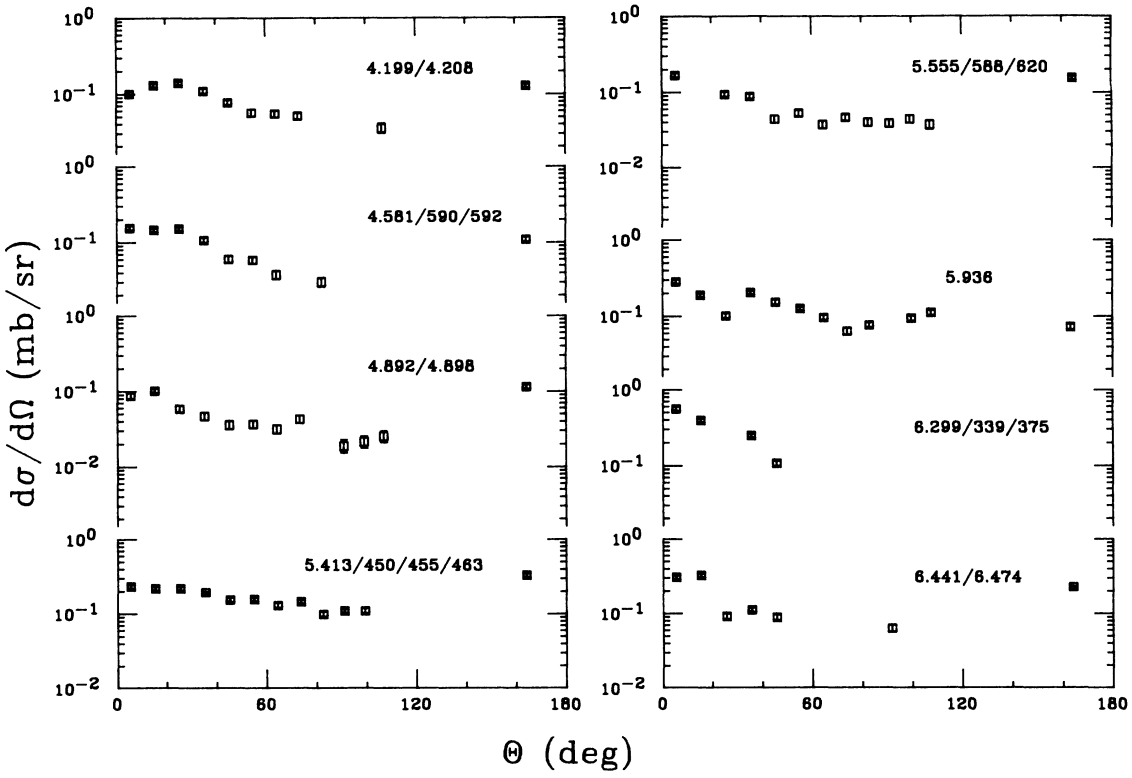

FIG. 7. Angular distributions for ^{20}F states with unknown J_π.

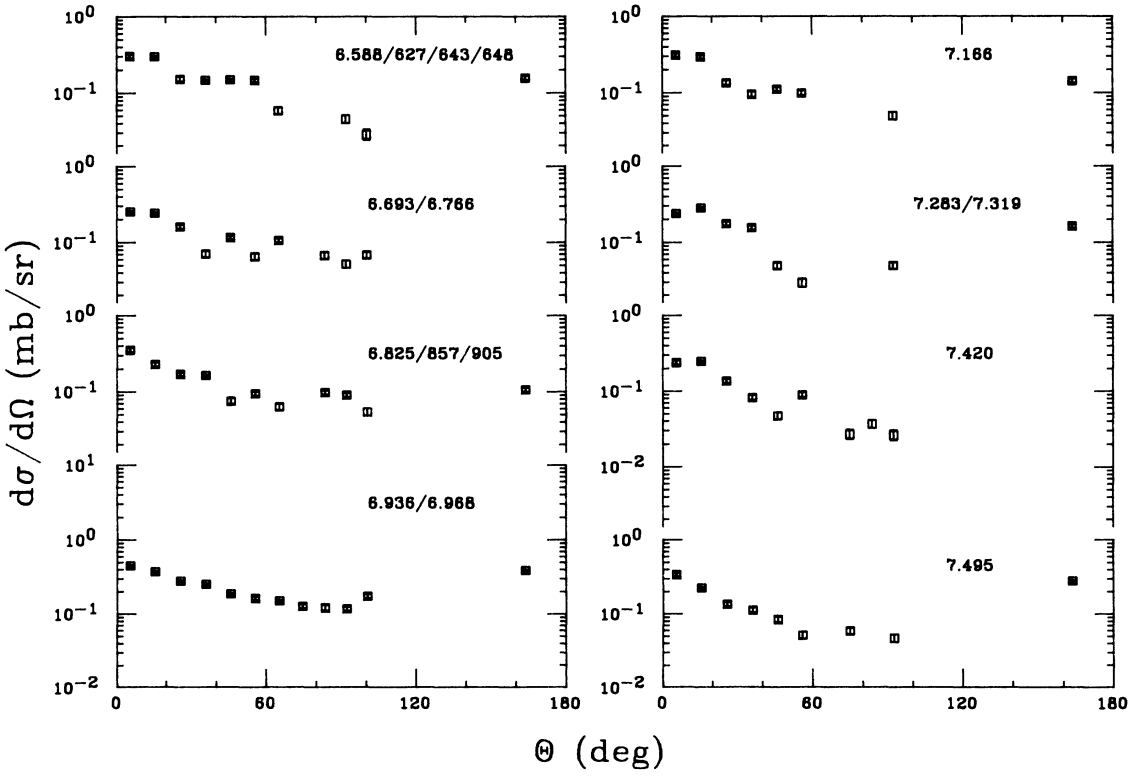

FIG. 8. Same as Fig. 7, but for $E_x = 6.5$–7.4 MeV.

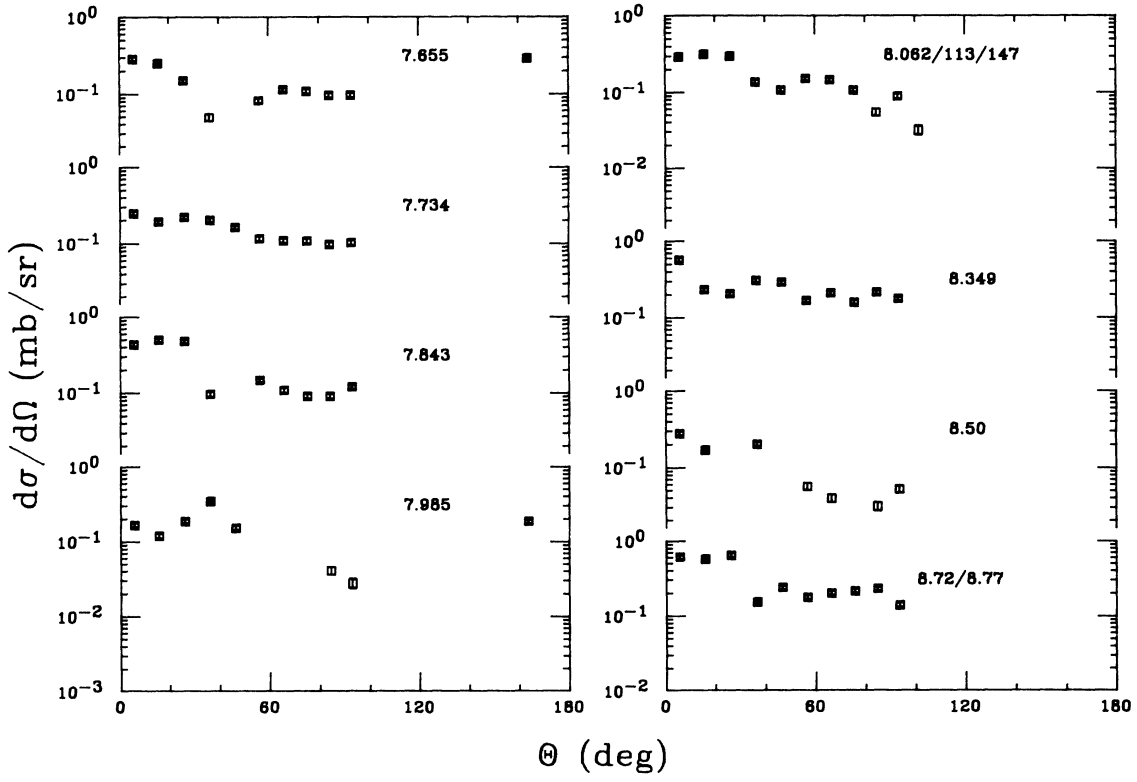

FIG. 9. Same as Fig. 7, but for $E_x = 7.4$–8.7 MeV.

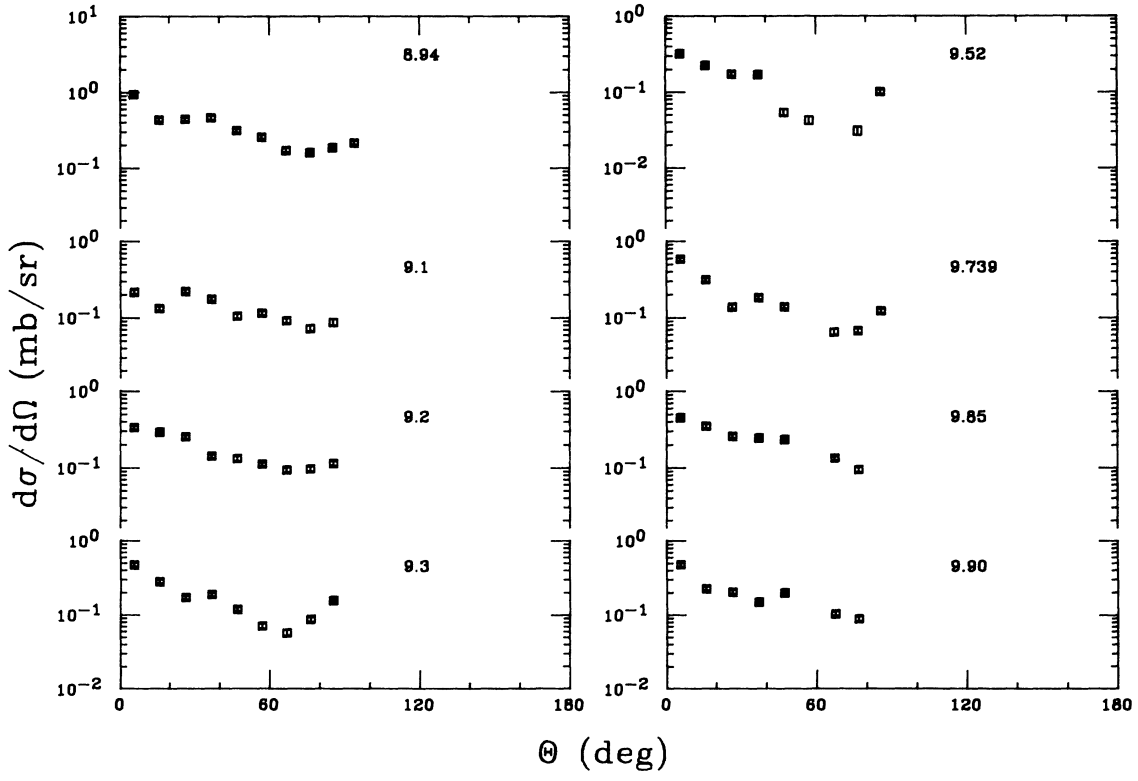

FIG. 10. Same as Fig. 7, but for $E_x = 8.9$–9.9 MeV.

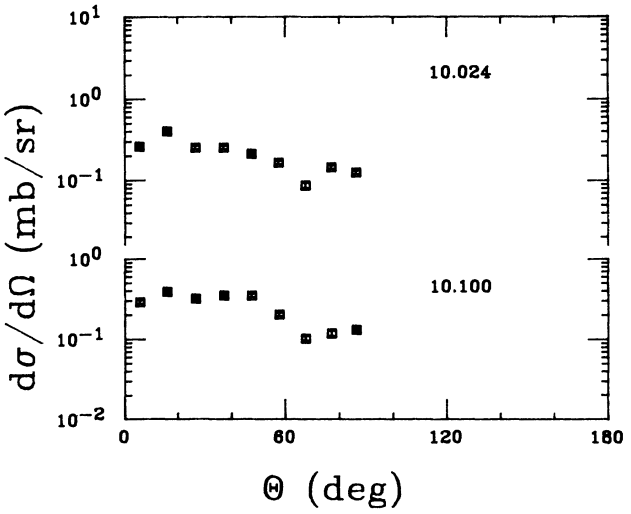

FIG. 11. Same as Fig. 7, but for $E_x = 10.0-10.1$ MeV.

some of these reactions have been analyzed by using the statistical model.[27]

The compound-nuclear decay channels used in the calculations of the present reaction are $^{13}C+^{11}B$, $\alpha+^{20}F$, $n+^{23}Na$, $p+^{23}Ne$, $d+^{22}Ne$, and $t+^{21}Ne$. Integrated cross sections σ_{HF} from HF calculations are listed in Table I for all states with known J^π. Angular distributions of states with known J^π are compared with HF calculations in Figs. 3–6. From these figures, we see that HF calculations provide a reasonable description of the experimental angular distributions for most of the identified states with known J^π.

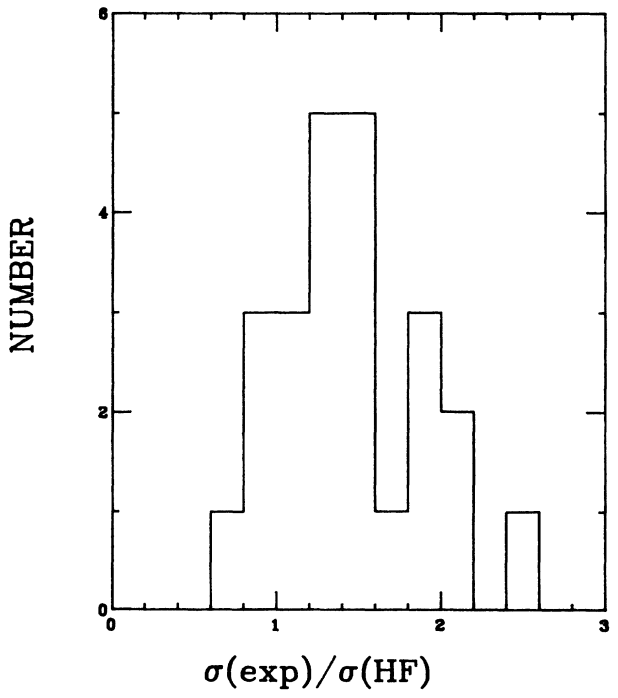

FIG. 12. A frequency distribution of σ_{exp}/σ_{HF} for the states of ^{20}F with identified J^π.

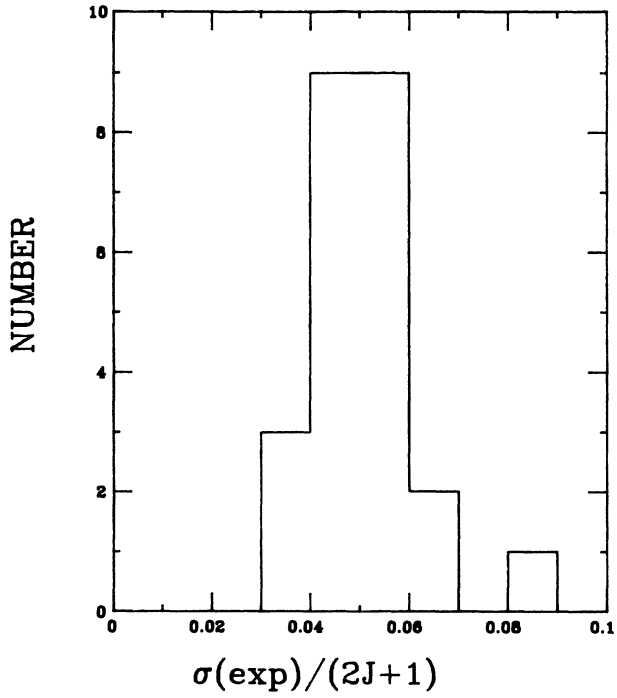

FIG. 13. A frequency distribution of $\sigma_{exp}/(2J+1)$ for the states of ^{20}F with identified J^π.

In Figs. 7–11 angular distributions for states with unknown J^π are displayed. Most of these states are doublets or multiplets. Figure 12 contains a frequency distribution of σ_{exp}/σ_{HF} for all states with identified J^π. The average value of σ_{exp}/σ_{HF} is 1.46, with a standard deviation of 0.087. The distribution is quite broad, with a second maximum near $\sigma_{exp}/\sigma_{HF}=2$. One state (the one at 4.082 MeV) has a ratio larger than 2.2. This agreement in absolute cross sections is about as good as is expected. The deviations may correspond to individual fluctuations, as the STATIS calculations are for energy-averaged cross sections, and we have data at a single energy. We later construct angular distributions summed over excitation energy.

TABLE II. Calculated excitation energies in ^{20}F of the lowest state of each weak-coupling configuration.

Label	Configuration	J^π	E_x (MeV)
$^{21}Ne\otimes^{15}N$	$(sd)^5_{3/2^+}(1p)^{-1}_{1/2^-}$	$1^-,2^-$	1.363
$^{22}Ne\otimes^{14}N$	$(sd)^6_{0^+}(1p)^{-2}_{1^+}$	1^+	2.831
$^{22}Na\otimes^{14}C$	$(sd)^6_{3^+}(1p)^{-2}_{0^+}$	3^+	5.110
$^{23}Na\otimes^{13}C$	$(sd)^7_{3/2^+}(1p)^{-3}_{1/2^-}$	$1^-,2^-$	4.669
$^{24}Na\otimes^{12}C$	$(sd)^8_{4^+}(1p)^{-4}_{0^+}$	4^+	4.856

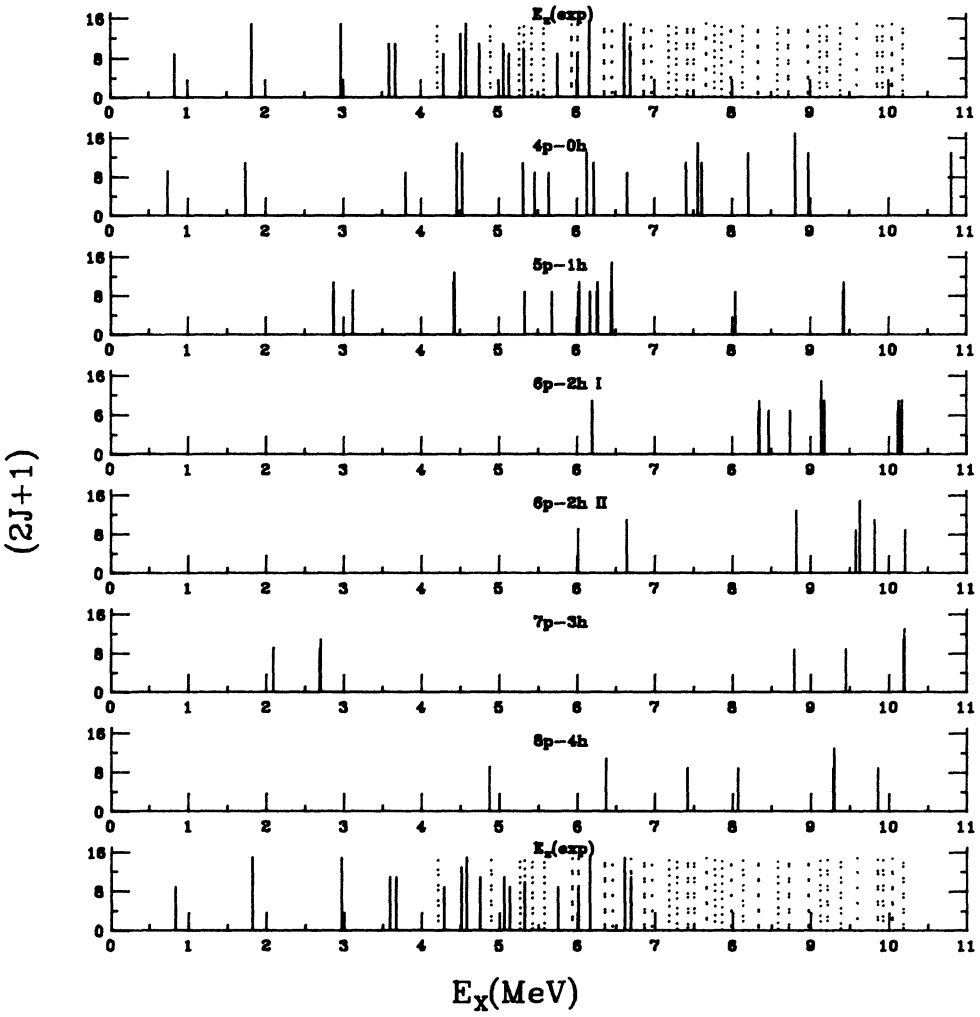

FIG. 14. Distributions of high-spin states ($J \geq 4$) from weak-coupling configurations of 4p-0h, 5p-1h, 6p-2h, 7p-3h, and 8p-4h compared with the experimental states, solid lines for the states with known J^{π} and dot lines for the states with unknown J^{π}.

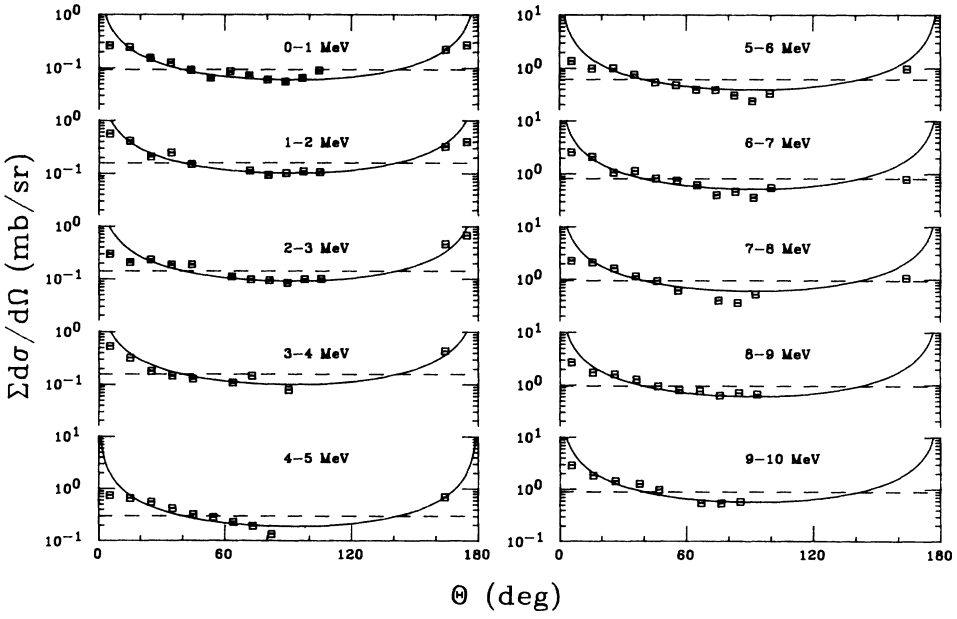

FIG. 15. Summed differential cross section per MeV, $\sum d\sigma/d\Omega$ vs θ.

As good as the agreement is between data and HF calculations, our σ_{exp} appear to be even better correlated with $2J+1$. In Fig. 13 we show a frequency distribution of $\sigma_{exp}/(2J+1)$. We find that the distribution of $\sigma_{exp}/(2J+1)$ is roughly peaked around $\sigma_{exp}/(2J+1)=0.05$ and is even narrower than that in Fig. 12. Based on this distribution, we calculate its average $R=\langle\sigma_{exp}/(2J+1)\rangle=0.048$, and its standard deviation $\delta R=0.0086$. Then we compute angular momentum limits $J\pm\delta J$ for each state, using the equation $J=(\sigma_{exp}/2R)-\frac{1}{2}$. In the fifth column of the Table I, we list $J\pm\delta J$ from this computation.

Up to 4.1 MeV excitation, the results of this procedure agree with the known J in 18 of 19 cases—the sole exception being the 1.97-MeV 3^- state. The reason for this discrepancy is not known, but we do note the nearby presence of an impurity peak [the ^{19}F ($\frac{5}{2}^+$; 0.197 MeV) state].

The quantity $J\pm\delta J$ allows us to identify candidates for states with high J. Calculation of excitation energies of weak-coupling configurations[28] have been carried out. Table II lists the results for the lowest state of each weak-coupling configuration. In Fig. 14, E_x distributions of high-J states ($J\geq 4$) from the configurations[14] of 4p-0h, 5p-1h, 6p-2h, 7p-3h, and 8p-4h are shown together with experimental results. Dotted lines there are for experimental states with unknown J^π. Comparing the experimental results of J limits with expected locations of high-spin states, we get the impression that many of the predicted high-spin states are populated in the present experiment. For example, the newest compilation[18] lists a state at 4.509 MeV with $J^\pi=1^+(2)$. However, considering the present result for the J limit and HF calculations and for Wildenthal's calculation of $(sd)^4$ states,[19] we prefer a state at 4.511 with 6^+ or 4^- from Ref. 13.

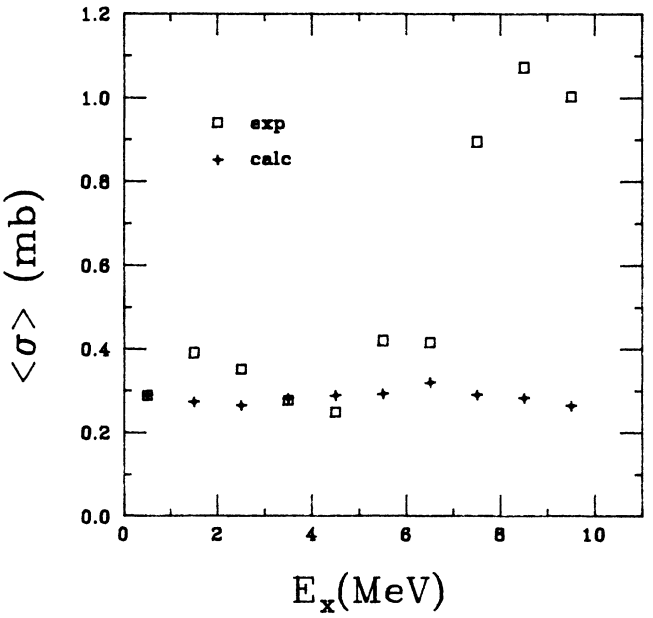

FIG. 17. A plot of summed integrated cross section divided by number of known states per MeV, $\langle\sigma\rangle$ vs E_x.

The compilation shows two states at 4.581 and 4.592 MeV, and we observe a peak at 4.577 MeV. Wildenthal in the same calculation predicted a state at 4.458 MeV with $J^\pi=7^+$. Comparing our J limit and HF calculations for our 4.577-MeV state with Wildenthal's prediction, we think the 4.577-MeV state might be the state with $J^\pi=7^+$. Earlier work[13,14] had already suggested

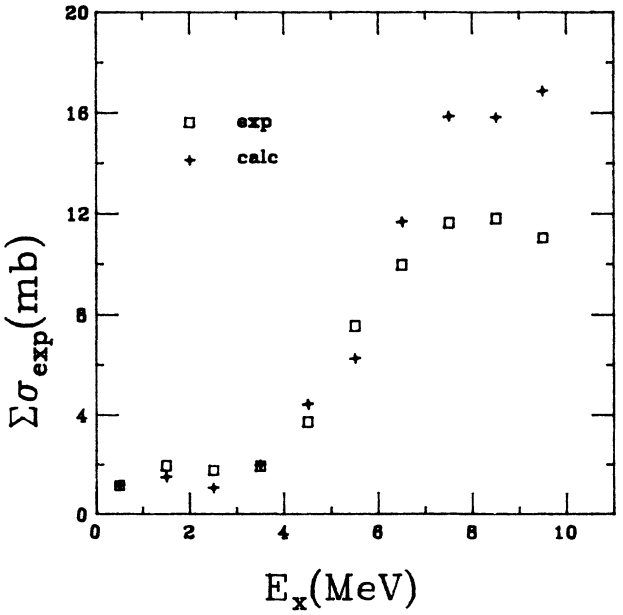

FIG. 16. A plot of summed integrated cross section per MeV, $\Sigma\sigma_{exp}$ vs excitation energy E_x.

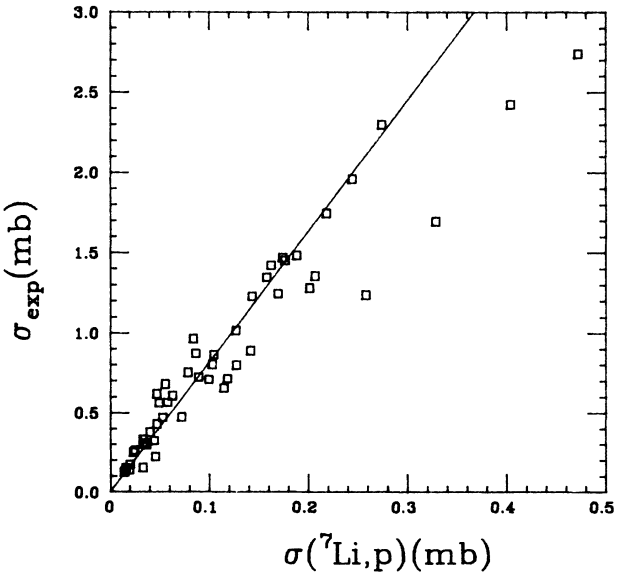

FIG. 18. A plot of cross section σ_{exp} from ^{13}C(^{11}B,α)^{20}F vs cross section $\sigma(^7\text{Li},p)$ from ^{14}N(^{7}Li,p)^{20}F for all states up to 8.5 MeV.

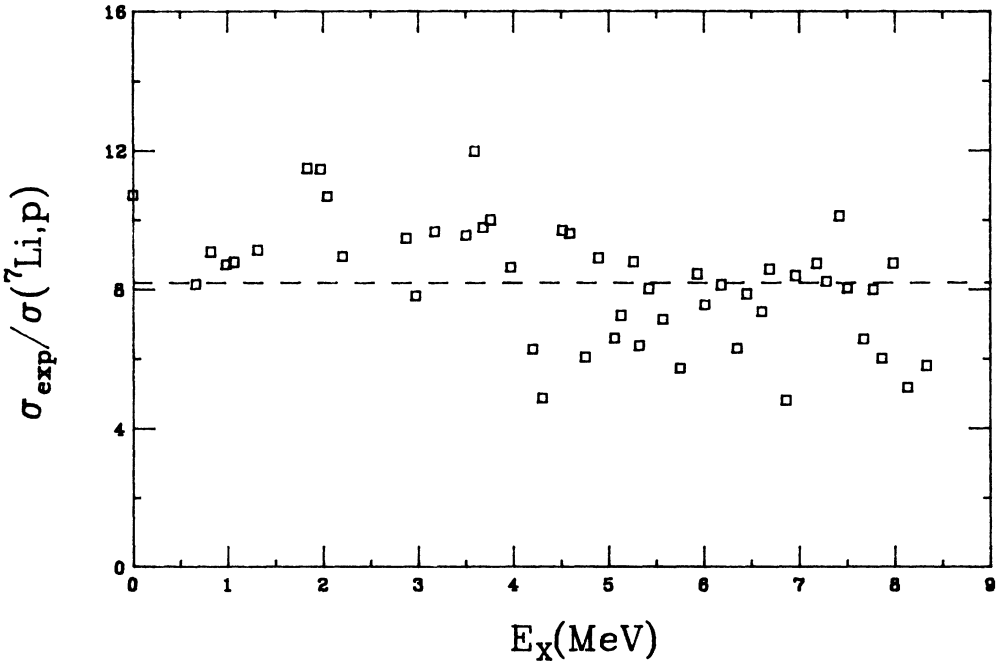

FIG. 19. A plot of ratio $\sigma_{exp}/\sigma(^7\text{Li},p)$ vs E_x.

high spin ($J \geq 4$) for a state at 4.59 MeV, which is undoubtedly the same state. The present work observes a state at 5.934 MeV, which is very close to the 5.936-MeV state listed as 2^- in the recent compilation.[18] However, our result has a J limit not less than 11 for a single state. This result is consistent with Ref. 14, which suggests a J limit of 11.3 ± 1.3. Because no such high-spin state is expected at this excitation from weak-coupling configurations, we expect it may be a doublet or triplet, including a 2^- state.

We will not discuss each one, but our extracted $J \pm \delta J$ is in disagreement with the compiled J value for many

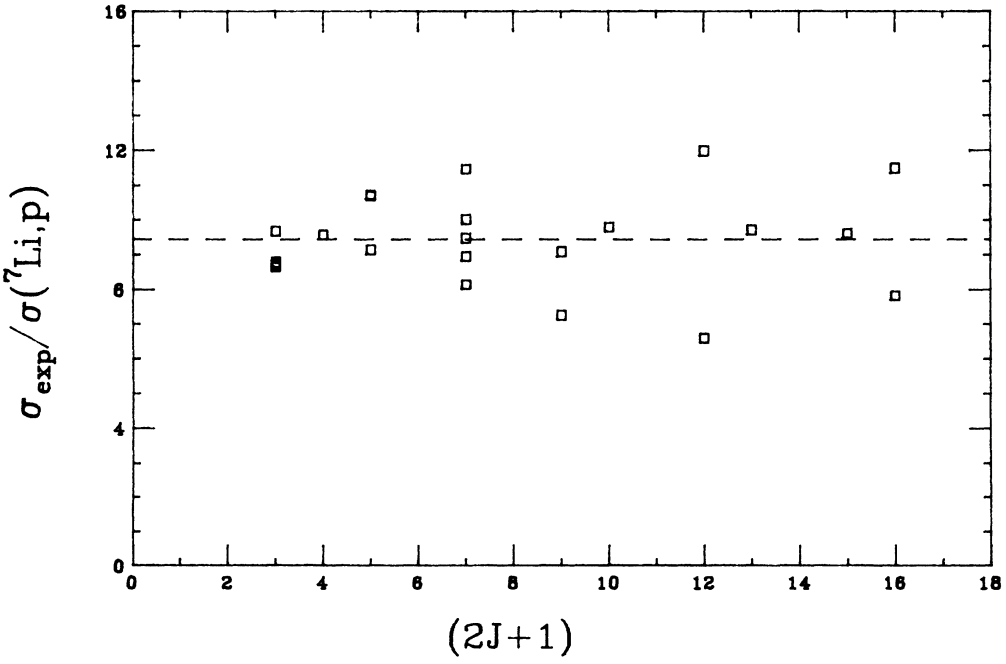

FIG. 20. A plot of ratio $\sigma_{exp}/\sigma(^7\text{Li},p)$ vs $(2J+1)$ for states with identified J^π.

states—always in the direction of being larger than expected. Because most of the predicted high-J states above 5 MeV have not been observed, and because most of the J^π assignments in the compilation for this energy region come from reactions that selectively excite low-J states, we do not question the existing low-J assignments. Rather, we suggest in such cases that both states may be present—the previously known low-J one and the new high-J one. We note that the number of such cases between 5 and 8 MeV is 17. The number of expected states in this region with $J \geq 5$ is 15.

In Fig. 15 we display summed differential cross sections per MeV, $\sum d\sigma/d\Omega$, together with their averages (dashed-straight lines) and curves $k/\sin\theta$ (solid curves), with k chosen to give the observed angle-integrated cross sections. From the figure one notes that most data points lie between the two curves.

In Fig. 16 we plot the summed integrated cross sections $\sum\sigma_{\text{exp}}$ vs excitation energies E_x and Fig. 17 displays the summed integrated cross sections divided by the numbers of *known* states per MeV: $\langle\sigma\rangle = (\sum\sigma_{\text{exp}}/\text{number of state})$ vs E_x. From Fig. 17, we find that below 7 MeV, $\langle\sigma\rangle$ is approximately constant, and then it increases rapidly. This fact means several states have not yet been identified at excitation energies higher than 7 MeV. This point is made even more clear when we compare with expected cross sections. The + symbols in Fig. 16 were obtained by multiplying our measured value of $\sigma_{\text{exp}}/(2J+1)$ times the sum of $2J+1$ values for *predicted* states in the various 1-MeV bins. In Fig. 17 the squares are the measured cross sections divided by the number of *known* states, while the +'s represent the calculated value of the same quantity, but for the *expected* number of states. It is quite obvious that the denominator for the squares is too low, i.e., many states remain to be identified above about 7 MeV.

IV. COMPARISON WITH RESULTS OF THE ^{14}N(^{7}Li,p)^{20}F REACTION

A plot of cross sections σ_{exp} from the present ^{13}C(^{11}B,α)^{20}F reaction vs $\sigma(^7\text{Li},p)$ from the ^{14}N(^{7}Li,p)^{20}F reaction is shown in Fig. 18 for the final states of ^{20}F up to 8.5 MeV. These are all normalized so that they correspond to 0°–180° cross sections. The straight line represents the average ratio of the two reaction cross sections. Most points are scattered around the straight line, and only a few points spread far away from it. The correlation coefficient between cross sections in the two reactions is 0.88.

Figure 19 is a plot of the ratio $\sigma_{\text{exp}}/\sigma(^7\text{Li},p)$ vs excitation energy E_x. Figure 20 displays $\sigma_{\text{exp}}/\sigma(^7\text{Li},p)$ vs $(2J+1)$ for each state with known J value. The points in Fig. 19 cluster near a horizontal line, but with a slight indication of a decrease with increasing E_x—i.e., a slight decrease of ^{13}C(^{11}B,α) cross section with E_x. A hint of such a decrease may be noted also in Fig. 16 and is not unexpected for such a wide range of E_x. (The $\alpha+^{20}$F Coulomb barrier is about 5 MeV, the outgoing α center-of-mass energy for $E_x=8$ MeV is 11.1 MeV.) Figure 20 indicates no systematic trend in the ratio—implying that J selectivity is very similar in the two reactions.

TABLE III. Grazing angular momentum l_{gr} for the entrance and exit channels.

Channel	^{13}C(^{11}B,α)^{20}F	^{14}N(^{7}Li,p)^{20}F
Entrance	9.3	7.3
Exit (0.0 MeV)	8.7	4.0
Exit (10.0 MeV)	6.4	2.9

Table III shows the grazing angular momenta l_{gr} for ^{13}C(^{11}B,α)^{20}F at $E_{\text{lab}}=22.0$ MeV and l'_{gr} of ^{14}N(^{7}Li,p)^{20}F at $E_{\text{lab}}=16.0$ MeV for both entrance channel and exit channels. Classically, the reaction cross section is proportional to l_{gr}^2. Here the value $(l_{\text{gr}}/l'_{\text{gr}})^2_{\text{ent}}*(l_{\text{gr}}/l'_{\text{gr}})^2_{\text{exit}}$ is 7.7. This number is very close to the average ratio of the two reaction cross sections

$$\left\langle \frac{\sigma_{\text{exp}}}{\sigma(^7\text{Li},p)} \right\rangle = 8.17 \pm 0.25 \ .$$

V. CONCLUSION

In the present study of ^{13}C(^{11}B,α)^{20}F at 22.0 MeV, we have measured differential cross sections for 60 groups of states of ^{20}F up to 10.1 MeV. For most states with known J^π, HF calculations give reasonable fits for both angular distributions and integrated cross sections. As for the states with unknown J^π, our results give some limits on the possible J values. At high-excitation energies ($E_x \geq 5$ MeV), many low-J states must be unresolved from nonidentified high-J states, because of relatively bad resolution. Comparison between results from this reaction and those from the ^{14}N(^{7}Li,p)^{20}F reaction shows that the cross sections of the two reactions are tightly correlated. The J selectivity of the two reactions is very similar, and the average ratio between the two is in good agreement with the ratio expected from quite simple arguments concerning grazing angular momentum. Finally, weak-coupling calculations for $(4+n)$p-nh states ($n=0$–4) provide a general guide to the high-spin states with $J \geq 4$.

[1]H. T. Fortune, J. D. Garrett, J. R. Powers, and R. Middleton, Phys. Rev. C **4**, 850 (1971).
[2]J. V. Maher, H. T. Fortune, G. C. Morrison, and B. Zeidman, Phys. Rev. C **5**, 1313 (1972).
[3]H. T. Fortune and R. R. Betts, Phys. Rev. C **10**, 1292 (1974).
[4]D. J. Crozier and H. T. Fortune, Phys. Rev. C **10**, 1697 (1974).
[5]G. F. Millington, J. R. Lealie, W. Mclatchie, G. C. Ball, W. G. Davis, and J. S. Forster, Nucl. Phys. **A228**, 382 (1974).
[6]R. Medoff, L. R. Medsker, S. C. Headley, and H. T. Fortune, Phys. Rev. C **14**, 1 (1976).

[7]C. A. Mosley, Jr. and H. T. Fortune, Phys. Rev. C **16**, 1697 (1977).
[8]F. Ajzenberg-Selove, Nucl. Phys. **A300**, 1 (1978).
[9]J. C. Hardy, H. Brunnarder, and J. Cerny, Phys. Rev. Lett. **22**, 1439 (1969).
[10]F. Ajzenberg-Selove, Nucl. Phys. **A382**, 1 (1983).
[11]H. T. Fortune and J. D. Garrett, Phys. Rev. C **14**, 1695 (1976).
[12]J. N. Bishop and H. T. Fortune, Phys. Rev. Lett. **34** 1350 (1975).
[13]H. T. Fortune and J. N. Bishop, Nucl. Phys. **A293**, 221 (1977).
[14]H. T. Fortune and R. Eckman, Phys. Rev. C **31**, 2076 (1985).
[15]K. Bodek *et al.*, J. Phys. G **6**, 1017 (1980).
[16]J. C. Legg, D. J. Crozier, G. G. Seaman, and H. T. Fortune, Phys. Rev. C **18**, 2202 (1978).
[17]H. T. Fortune and J. N. Bishop, Nucl. Phys. **A304**, 221 (1978).
[18]F. Ajzenberg-Selove, Nucl. Phys. **A475**, 1 (1987).
[19]B. H. Wildenthal, private communication.
[20]G.-B. Liu and H. T. Fortune, Phys. Rev. C **37**, 1818 (1988).
[21]P. R. Bevington, *Data Reduction and Analysis for the Physical Sciences* (McGraw-Hill, New York, 1969).
[22]R. G. Stokstad, the code STATIS Internal Report 52, Wright Nuclear Structure Laboratory, Yale University, 1972 (unpublished).
[23]W. Hauser and H. Feshback, Phys. Rev. **87**, 366 (1952).
[24]R. Middleton, J. D. Garret, and H. T. Fortune, Phys. Rev. C **4**, 1987 (1971).
[25]J. N. Hallock, H. A. Enge, A. Sperduto, R. Middleton, J. D. Garrett, and H. T. Fortune, Phys. Rev. C **6**, 2148 (1972).
[26]J. N. Hallock, H. A. Enge, A. Sperduto, J. D. Garrett, R. Middleton, and H. T. Fortune, Nucl. Phys. **A306**, 229 (1978).
[27]J. N. Hallock, H. A. Enge, J. D. Garrett, R. Middleton, and H. T. Fortune, Nucl. Phys. **A252**, 141 (1975).
[28]H. T. Fortune and B. H. Wildenthal, Phys. Rev. C **30**, 1063 (1984).